Large contribution of soil emissions to the atmospheric nitrogen budget and their impacts on air quality and temperature rise in North China

Tong Sha[1], Siyu Yang[1], Qingcai Chen[1], Liangqing Li[1], Xiaoyan Ma[2], Yan-Lin Zhang[3,4], Zhaozhong Feng[3], K. Folkert Boersma[5,6], Jun Wang[7*]*

[1] School of Environmental Science and Engineering, Shaanxi University of Science and Technology, Xi'an 710021, China

[2] Key Laboratory for Aerosol-Cloud-Precipitation of China Meteorological Administration, Nanjing University of Information Science & Technology, Nanjing 210044, China

[3] School of Ecology and Applied Meteorology, Nanjing University of Information Science & Technology, Nanjing 210044, China

[4] Atmospheric Environment Center, Joint Laboratory for International Cooperation on Climate and Environmental Change, Ministry of Education (ILCEC), Nanjing University of Information Science & Technology, Nanjing 210044, China

[5] Satellite Observations Department, Royal Netherlands Meteorological Institute, De Bilt 3731GA, the Netherlands

[6] Meteorology and Air Quality Group, Wageningen University, Wageningen 6708PB, the Netherlands

[7] Department of Chemical and Biochemical Engineering, Center for Global and Regional Environmental Research, and Iowa Technology Institute, University of Iowa, Iowa City, IA, 52242, USA

*Corresponding authors:

Tong Sha: tong-sha@sust.edu.cn

Jun Wang, jun-wang-1@uiowa.edu

Submitted: February 2024

Revised: June 2024

Abstract

Soil emissions of nitrogen compounds, including NO and HONO, play a significant role in atmospheric nitrogen budget. However, HONO has been overlooked in previous research on soil reactive nitrogen (Nr) emissions and their impacts on air quality in China. This study estimates both soil NO_x and HONO emissions (SNO_x and SHONO) in North China during July 2018 with an updated soil Nr emissions scheme in a chemical transport model, the Unified Inputs for WRF-Chem (UI-WRF-Chem). The effects of soil Nr emissions on O_3 pollution, air quality and temperature rise are also studied, with a focus on two key regions, Beijing-Tianjin-Hebei (BTH) and Fenwei Plain (FWP), known for high soil Nr and anthropogenic emissions. We find that the flux of SNO_x is nearly doubled those of SHONO; the monthly contributions of SNO_x and SHONO account for 37.3% and 13.5% of anthropogenic NO_x emissions in the BTH, and 29.2% and 19.2% in the FWP during July 2018, respectively. Soil Nr emissions have a significant impact on surface O_3 and nitrate, exceeding SNO_x or SHONO effects alone. On average, soil Nr emissions increase MDA8 O_3 by 16.9% and nitrate concentrations by 42.4% in the BTH, 17.2% for MDA8 O_3 and 42.7% for nitrate in the FWP. Reducing anthropogenic NO_x emissions leads to a more substantial suppressive effect of soil Nr emissions on O_3 mitigation, particularly in BTH. Soil Nr emissions, via their role as precursors for secondary inorganic aerosols, can result in a slower increase rate of surface air temperature under future emission reduction scenarios. This study suggests that mitigating O_3 pollution and addressing climate change in China should consider the role of soil Nr emission, and their regional differences.

1. Introduction

Surface ozone (O_3) is a major air pollutant harmful to human health, terrestrial vegetation, and crop growth (Feng et al., 2022b; Turner et al., 2016; Unger et al., 2020; Yue et al., 2017). China is confronting serious O_3 pollution, with the surface O_3 concentrations routinely exceeding air quality standards (Li et al., 2019). Although the Chinese Action Plan on Air Pollution Prevention and Control implemented in 2013 has significantly reduced the nationwide anthropogenic emissions of primary pollutants including particulate matter (PM) and nitrogen oxides (NO_x = NO + NO_2), the summertime O_3 concentrations observed by national ground sites and satellite observations both show an increasing trend of 1-3 ppbv a^{-1} in megacity clusters of eastern China from 2013 to 2019 (Wang et al., 2022b; Wei et al., 2022). Many studies have explored the causes of O_3 pollution from the perspective of changes in meteorology and anthropogenic emissions, and attributed the O_3 increase to decreased PM levels and anthropogenic NO_x emissions, and adverse meteorological conditions (Li et al., 2019; Li et al., 2020; Li et al., 2021b; Liu and Wang, 2020a, b; Lu et al., 2019).

Soil emissions are an important natural source of reactive nitrogen species, including N_2O, NO_x, HONO and NH_3, and can strongly affect the atmospheric chemistry, air pollution and climate change (Elshorbany et al., 2012; Pinder et al., 2012). It has been acknowledged that the soils emissions account for 12-20% of total emissions of NO_x on global average (Vinken et al., 2014; Yan et al., 2005), and 40-51% in agricultural regions during periods in which fertilizers are applied to soils, resulting in a significant increase in O_3 and NO_2 concentrations in US (Almaraz et al., 2018; Romer

et al., 2018; Sha et al., 2021; Wang et al., 2021a), Europe (Skiba et al., 2020) and sub-Saharan Africa (Huang et al., 2018).

China has a large area of cultivated land (~1.276 $\times 10^6$ km^2, http://gi.mnr.gov.cn/202304/t20230414_2781724.html, last access: 18th December 2023), which contributes to one-third of the global nitrogen fertilizer use and has extensive nitrogen deposition (Liu et al., 2013; Lu and Tian, 2017; Reay, 2008). So far, only a limited studies focused on the impact of soil NO_x emissions (denoted as SNO_x) on O_3 pollution in China (Huang et al., 2023; Lu et al., 2021; Shen et al., 2023; Wang et al., 2008; Wang et al., 2022a; Wang et al., 2023a). Lu et al. (2021) demonstrated that the presence of SNO_x in the North China Plain significantly reduced the sensitivity of surface O_3 to anthropogenic emissions. Huang et al. (2023) suggested that substantial SNO_x could increase the maximum daily 8 h (MDA8) O_3 concentrations by 8.0–12.5 μg m^{-3} on average for June 2018 in China. These studies focused only on NO_x emitted from soils and neglected that similar soil microbial activities also emit nitrous acid (HONO). The measurements in laboratory showed that the emission rates of soil HONO were comparable to those of NO (Oswald et al., 2013; Weber B, 2015). The photolysis of HONO has been identified to be an important source of atmospheric hydroxyl radical (·OH), which enhances concentrations of hydroperoxyl (HO_2) and organic peroxy radicals (RO_2), accelerating the conversion of NO to NO_2, resulting in more concentrations of O_3 and secondary pollutants. Although the sources and formation mechanisms of HONO are still not fully understood, recent model studies suggested that HONO emission from soils in the agriculture-intensive North China Plain could

increase the regionally averaged daytime ·OH, O_3, and daily fine particulate nitrate concentrations (Feng et al., 2022a; Wang et al., 2021b).

Only a few studies simultaneously considered the impact of soil HONO emissions (denoted as SHONO) along with SNO_x on O_3 and other secondary pollutants (Tan et al., 2023; Wang et al., 2023c). Wang et al. (2023c) found that the NO_x and HONO emissions from natural soils (i.e., soil background emissions) increased daily average O_3 concentrations by 2.0% in the Northeast Plain during August 2016 without considering the contribution from fertilized croplands. Tan et al. (2023) believed that the contribution of soil NO_x and HONO to O_3 pollution has been in an increasing trend from 2013 (5.0 pptv) to 2019 (8.0 pptv) in the summer season over the North China Plain by using the GEOS-Chem model; however the coarse resolution of GEOS-Chem simulation may not insufficient to resolve the spatial heterogeneity in soil emission distribution (Lu et al., 2021). Associated with the decreasing anthropogenic emissions is the increasing contribution of soil emissions to the atmospheric nitrogen budget in China. Therefore, it is critical to quantify the impact of soil reactive nitrogen (Nr: NO_x and HONO) emissions on O_3 and secondary pollutants.

In this study, we improve the soil Nr emissions scheme in the Unified Inputs (initial and boundary conditions) for Weather Research and Forecasting model coupled with Chemistry (UI-WRF-Chem) by considering all potential sources of HONO published in the literature. July 2018 was chosen as the study period because of severe O_3 pollution during this month, as well as higher air temperatures and more frequent precipitation compared to June and August (Figure S1 and S2), which could contribute

to enhanced the soil Nr emissions (Figure S3). We conduct a series of sensitivity experiments to quantify the coupled and separate impact of SNO_x and SHONO on O_3 and secondary pollutants during July 2018 over the North China, focusing on two city clusters, the Beijing-Tianjin-Hebei (BTH) region and Fenwei Plain (FWP) region, both of which have the vast areas of croplands and dense populations and experiencing severe O_3 and $PM_{2.5}$ pollutions. In addition, by quantitatively analyzing the difference in the response of surface O_3 concentrations and surface air temperature to the anthropogenic emissions reductions in the presence vs. absence of soil Nr emissions, the roles of soil Nr emissions on O_3 mitigation strategies and climate change are also studied. Our study is designed to address the underestimated role of soil Nr emission in O_3 pollution, thereby providing the scientific basis for O_3 mitigation strategies and climate change.

2. Methodology

2.1 Model description

2.1.1 Model configurations, input data, and non-soil HONO emission

The UI-WRF-Chem model, developed upon the standard version of WRF-Chem 3.8.1 (Grell et al., 2005), was used in this study. The 0.625°×0.5° Modern-Era Retrospective analysis for Research and Applications, Version 2 (MERRA-2) reanalysis data provide both the meteorological and chemical boundary and initial conditions (Gelaro et al., 2017). The 0.25° × 0.25° Global Land Data Assimilation System (GLDAS) data provides the initial and boundary conditions of soil properties, i.e., soil moisture and temperature (Rodell et al., 2004). Details of Unified Inputs of

meteorological and chemical position data for UI-WRF-Chem, can be found in recent publications (Li et al., 2024; Wang et al., 2023d). Anthropogenic emissions are imported from the Multi-resolution Emission Inventory for China (MEIC: http://www.meicmodel.org/) with a spatial resolution of 0.25° × 0.25° for the year 2017. Due to the differences in spatial resolution and map projection between the MEIC inventory and model grid, we applied a spatial interpolation method to convert the MEIC inventory to the model-ready formats. The descriptions are detailed in Text S1. Biomass burning emissions are from the Fire Inventory from NCAR version (FINN, version 1.5, https://www.acom.ucar.edu/Data/fire/). Biogenic emissions are calculated using the Model of Emissions of Gases and Aerosols from Nature (MEGAN) version 2.1 (Guenther et al., 2012).

The physical and chemical schemes include the Morrison 2-moment microphysical scheme (Morrison et al., 2009), Grell 3-D cumulus scheme (Grell and Dévényi, 2002), RRTMG for both longwave and shortwave radiation scheme (Iacono et al., 2008), Yonsei University planetary boundary layer scheme (Hong et al., 2006), Noah land surface model (Tewari et al., 2004), and the Carbon Bond Mechanism (CBMZ) for gas-phase chemistry and the Model for Simulating Aerosol Interactions and Chemistry (MOSAIC) aerosol module with four sectional aerosol bins and aqueous reactions (Zaveri and Peters, 1999; Zaveri et al., 2008) are adopted in the UI-WRF-Chem model. Two nested domains are used, domain one covers China with a horizontal resolution of 27 km and contains 112×112 grid cells, and domain two covers central and eastern China and its surrounding area with a horizontal resolution of 9 km,

containing 196×166 grid cells (study region are shown in Figure S4), both domains have 74 vertical levels from surface to 50 hPa and 4 levels of soil. The simulations are conducted from 29th June to 31th July in 2018 with the first 2 days as the spin-up period. The model outputs from 1th to 31th July in 2018 are analyzed.

The default WRF-Chem model only considers the gas-phase formation of HONO ($NO + OH \rightarrow HONO$), thus underestimating the HONO concentrations. In this study, in addition to considering SHONO (details in Section 2.1.2), potential sources of HONO recognized in recent studies are also taken into account in the current model (Fu et al., 2019; Li et al., 2010; Ye et al., 2016; Ye et al., 2017; Zhang et al., 2016; Zhang et al., 2020; Zhang et al., 2021; Zhang et al., 2022a, b), including traffic emissions, NO_2 heterogeneous reactions on ground and aerosol surfaces, and inorganic nitrate photolysis in the atmosphere. Through a series of tests and comparisons with observed surface HONO concentrations, the specific parameterization schemes of HONO sources adopted in this study are shown in Text S2.

2.1.2 Parameterization of soil Nr emissions

The soil Nr emissions schemes in the UI-WRF-Chem model are updated in this study. The default SNO_x scheme in UI-WRF-Chem, MEGAN v2.1, is replaced by the Berkeley−Dalhousie−Iowa Soil NO Parameterization (BDISNP), and the implementation of BDISNP can be found in Sha et al. (2021). Considering that the baseline year of N fertilizer data is 2006, and the amount of N fertilizer application in China has changed in the past ten years, we update the N fertilizer data to the year 2018 based on the N fertilizer application data at the province level from the statistical

yearbook (Table S1).

The process of soil HONO emission is similar to that of NO_x, as both are influenced by the physical and chemical characteristics of soils. Consequently, soil emissions of HONO with consideration of their dependence on land type, soil humidity, and temperature are also parameterized into the UI-WRF-Chem model. We first map the soil types measured in Oswald et al. (2013) (collected from 17 ecosystems in Table S2) into the most closely matching MODIS land cover types in the model following Feng et al. (2022a), described in Table S3. The optimal emission flux for each MODIS land cover type is calculated as the average of the measured fluxes from the category/categories in Oswald et al. (2013) that is/are been mapped into a specific MODIS classification. We also collect the SHONO data from various ecosystems in China published in different studies to correct the optimal SHONO fluxes in the model (Table S4). These ecosystems include semi-arid, fertilized and irrigated farmland in China. Consequently, the parameterization scheme takes into account the effect of fertilizer application on the SHONO. After that, the optimal fluxes over the domains are digested into the model and further scaled online according to the soil temperature and water content in each model grid at each time step throughout the simulation period by the following of equation from (Zhang et al., 2016):

$$F_N(\mathrm{HONO}) = F_{N,opt}(\mathrm{HONO}) \cdot f(T) \cdot f(SWC)$$

where $F_{N,opt}(\mathrm{HONO})$ is the optimum flux of SHONO in terms of nitrogen. $f(T)$ and $f(SWC)$ are the scaling factors of soil temperature (T) and water content (SWC).

$$f(T) = e^{\frac{Ea}{R}(\frac{T}{T_{opt}}-\frac{1}{T})}$$

E_a is the activation energy of HONO (80 kJ mol^{-1}), R is the gas constant, T_{opt} is the temperature at which optimum flux is emitted (298.15 K), T is the soil temperature calculated online by the model, $f(SWC)$ is fitted based on the data curves in Figures 1 and 3 in (Oswald et al., 2013) and the equation is as follows:

$$f(SWC) = 1.04 \times exp^{(-e^{-\frac{SWC-11.32586}{5.27335}}-\frac{SWC-11.32586}{5.27335}+1)}$$

2.2 Model experiment design

The descriptions of the sensitivity simulations are shown in Table 1. Default simulation uses MEGAN scheme to estimate SNO_x and no SHONO is considered. Base simulation uses soil Nr emissions schemes with the improvement of using BDISNP scheme for SNO_x and consideration of SHONO and other four HONO sources (as described above). Comparison of results from Default and Base simulations is used to show the improvement in the model performance after updating the soil Nr emissions schemes and incorporating HONO potential sources. To explore the impact of soil Nr emissions on O_3 and secondary pollutants, we conduct a series of sensitivity simulations with soil NO_x and HONO emissions turned on/off separately and jointly (anthropogenic emissions for the year 2017), i.e., NoSoilNr, NoSHONO and NoSNO_x. To investigate the relative importance and interaction between anthropogenic and natural emissions of nitrogen-containing pollutants, we conduct the Base_redANO_x and NoSoil_redANO_x simulations to evaluate the role of soil Nr emissions on O_3 mitigation strategies, in which anthropogenic NO_x emissions reduced by 20%, 40%, 60%, 80%, and 100%, respectively. Furthermore, considering the co-control of multiple air pollutants and greenhouse gas reductions in future emission reduction scenarios, the Base_redAnt and

NoSoil_redAnt simulations are conducted to evaluate the role of soil Nr emissions on air temperature change, and the anthropogenic reduction scenarios simultaneously consider SO_2, NO_x, primary $PM_{2.5}$, VOCs, and CO emissions reductions (reduced by 20%, 40%, 60%, 80%, and 100%).

2.3 Observational data

The tropospheric column densities of NO_2 from TROPOMI (TROPOspheric Monitoring Instrument) level-2 in version 1 with the horizontal spatial resolution of 3.5 × 7 km^2 are used (Van Geffen et al., 2021). The quality controls, i.e., cloud-screened (cloud fraction below 30%) and quality-assured (qa_value above 0.50), and averaging kernels (AK) are applied in the comparison of the TROPOMI and UI-WRF-Chem simulated tropospheric NO_2 vertical column densities (defined as NO_2 VCD).

To evaluate the model performance on simulating surface air pollutants, we use the hourly surface O_3 concentrations at 888 monitoring sites from the China National Environmental Monitoring Center (CNEMC), and hourly surface HONO concentrations measured by the In-situ Gas and Aerosol Compositions monitor (IGAC) (Zhan et al., 2021) at Nanjing University of Information Science & Technology (NUIST) (32.2º N, 118.7º E; 22m above sea level) (Xu et al., 2019).

3. Results and discussions

3.1 Soil nitrogen emissions and air pollution evaluation

The soil Nr emissions in July are much higher than the other seasons due to higher air temperatures and frequent precipitation, accounting for 39.5% of anthropogenic NO_x emissions over the study region, and 50.2% in the BTH, 47.4% in FWP, which is

consistent with the previous studies (Huang et al., 2023; Shen et al., 2023; Wang et al., 2023c). And the proportions can increase to 58.9%, 57.0%, and 65.0%, respectively, when only statistics over the cropland in these regions (Figure S3). Given the substantial contribution of soil emissions to the atmospheric nitrogen budget in July, we thus choose this month to assess the impact of soil Nr emissions on air quality and climate change. From the spatial distribution of simulated monthly mean SNO_x and SHONO fluxes across North China in July 2018 (Figure 1), it is shown that SNO_x flux is nearly doubled that of SHONO in most regions, and higher SNO_x and SHONO are concentrated in areas dominated by cropland. The monthly total soil emissions over the whole study domain (cropland) are 104.5 (82.4) Gg N mon^{-1} for NO_x and 52.7 (45.9) Gg N mon^{-1} for HONO. In the densely populated BTH region, the monthly total SNO_x are 18.7 Gg N mon^{-1} in July, which is equivalent to 37.3% of anthropogenic NO_x emissions for the year 2017. For the FEW region, where also experiences severe O_3 and $PM_{2.5}$ pollutions, the monthly total SNO_x (7.0 Gg N mon^{-1}) account for 29.2% of anthropogenic NO_x emissions. The monthly total SHONO in both study regions are much lower than their SNO_x counterparts, with the emissions of 6.9 and 4.6 Gg N mon^{-1}, accounting for 13.5% and 19.2% of anthropogenic NO_x emissions in BTH and FWP regions, respectively.

To evaluate the model performance, Figure 2 shows the tropospheric NO_2 VCD from TROPOMI satellite products and UI-WRF-Chem simulations (Default and Base) in North China during July 2018. Default and Base can both reproduce the hot spots of NO_2 VCD in urban areas shown in the TROPOMI observations. However, the Default

271 significantly underestimates the NO_2 VCD, especially in regions surrounding urban
272 areas. It is found that Default underestimates NO_2 VCD by 48% over the regions where
273 soil emissions dominate (i.e., soil Nr emissions contribute more than half to the
274 atmospheric nitrogen emissions), while the Base reduced the bias to 13% (Figure S5).
275 Overall, Base shows the improved performance in simulating NO_2 VCD in comparison
276 to Default with a decreasing bias from -30% (-21%) to +4% (+17%) and an increasing
277 spatial correlation coefficient (R) from 0.62 (0.50) to 0.65 (0.54) in the study region
278 (cropland). However, there is still a discrepancy between the Base simulation and
279 TROPOMI NO_2 VCD. This discrepancy could be driven by the combined effects from
280 uncertainties in simulations and observations, associated with the time lag in
281 anthropogenic emissions inventory used in the model (Chen et al., 2021), instantaneous
282 uncertainties in TROPOMI tropospheric NO_2 VCD at the pixel level (up to 25-50% or
283 $0.5\sim0.6\times10^{15}$ molecules cm^{-2}), as well as uncertainties of stratospheric portion of NO_2
284 VCD and AK caused the retrieval errors (Van Geffen et al., 2020; Van Geffen et al.,
285 2021). Additionally, the estimated SNO_x are also subjected to certain limitations and
286 uncertainties. The first uncertainty comes from the amount of N fertilizer application,
287 which has been identified as the dominant contributor to SNO_x. In this study, we use
288 the amount of agricultural N fertilizer application at the province level from the
289 statistical yearbook to update the default N fertilizer application data in the model (the
290 baseline year for 2006), but a recent study showed that compound fertilizer, usually
291 with nitrogen (N), phosphorus (P), and potassium (K), were more commonly used in
292 China; if only N fertilizer is considered to nudge the N fertilizer application data in the

model, the estimated SNO_x may be underestimated by 11.1%–41.5% (Huang et al., 2023). Furthermore, although we use the modeled green vegetation fraction (GVF) to determine the distribution of arid (GVF ≤ 30%) and non-arid (GVF > 30%) regions. Huber et al. (2023) showed that the estimated SNO_x based on the static classification of arid vs. non-arid is very sensitive to the soil moisture, and thus could not produce self-consistent results when using different input soil moisture products unless a normalized soil moisture index to represent. Therefore, more direct measurements of soil Nr fluxes are crucial to better constrain soil emissions and improve the parametrization in the model. Nevertheless, the improved simulation performance of NO_2 VCD with a reduced bias and increased spatial correlation coefficient in Base is credible, and soil Nr emission scheme has the fidelity needed to study the implication of soil Nr emissions to air quality in North China.

We evaluate the simulation with the surface O_3 observations from the China National Environmental Monitoring Centre (CNEMC) network (http://www.cnemc.cn/en/) (Figure 3). Over the whole study region, the Base can better capture the spatial distribution of observed surface MDA8 O_3 with a relatively higher spatial correlation of R = 0.68 than that in Default (R = 0.46). The simulated monthly averaged MDA8 O_3 concentrations across the 888 sites in the study region are 123.0 μg m^{-3} in Default and 132.5 μg m^{-3} in Base, respectively, which are both slightly higher than the observed concentrations (120.7 μg m^{-3}). Overprediction is also observed for the FWP and BTH regions in the Base simulation, with the normalized mean bias (NMB) of 6.1% and 4.9%, respectively (Figure S6). Previous studies showed that the NMB of

simulated O_3 concentrations were within ±30% for nearly 80% of the cases collected from air quality model studies (Yang and Zhao, 2023). These discrepancies may arise from simplifications of complex chemical mechanisms and physical processes, such as dry deposition and vertical mixing (Akimoto et al., 2019; Travis and Jacob, 2019). The uncertainties of input data, including emission inventories, meteorological fields, and other parameters, may also contribute to these discrepancies (Sun et al., 2019; Ye et al., 2022), suggesting a potential systematic O_3 bias in air quality models. Therefore, the increased spatial correlation and reasonable bias found in the Base indicate that the application of the soil Nr emission schemes can effectively improve the simulation performance of MDA8 O_3.

We also compare the simulated surface HONO and nitrate concentrations to the observations at a rural station in Nanjing during July 2018. Figure 4 shows that the simulated HONO concentrations in Default are 98.3% lower than the observations. In comparison, the Base with considering SHONO and other HONO potential sources significantly improves the simulation performance and reduces the bias to 47.8%, and also reproduces the diurnal variation of HONO with the temporal correlation of R = 0.76. It is worth noting that the simulated concentrations of HONO from 08 am to 18 pm are lower than the observations, this discrepancy may be attributed to the underestimated contribution from the predominant sources of HONO during the daytime, such as NO_2 heterogeneous reactions on ground and aerosol surfaces. Moreover, the contributions of different sources to ambient HONO concentrations at this rural station are also evaluated, the soil emissions could contribute almost 25.8%

to the surface HONO concentrations, which may be partially attributed to the high emissions of HONO from croplands around the city of Nanjing (Figure S7). The results that soil emissions contribute less to the daytime positive flux than the other source is consistent with previous studies (Skiba et al., 2020; Wang et al., 2023c). For nitrate concentration, the Base simulation shows a lower bias (5.6%) and an improved diurnal variation (temporal correlation of R = 0.92) compared to the Default simulation (bias = 27.8%, R = 0.85). We acknowledge that there are certain uncertainties in the current model. Nevertheless, the improved simulation performance of NO_2 VCD, surface HONO, MDA8 O_3, and nitrate concentrations compared to the Default illustrates the credibility of the results obtained from the Base simulation.

3.2 Impact on O_3 formation and air quality

To quantify the effects of SNO_x and SHONO on atmospheric oxidation capacity, O_3 formation and air quality as well as their combined effect, the conventional brute-force method was used, i.e., the impact of a specific source is determined in atmospheric chemistry models as the differences between the standard/base simulation with all emissions turned on and a sensitivity simulation with this source turned off or perturbed (Table 1). As shown in Figure 5, the contribution of SNO_x and SHONO to surface NO_2 and HONO has a different spatial pattern from that of the fluxes of SNO_x and SHONO in July. Overall, the maximum contribution of SNO_x to the monthly average surface NO_2 concentrations is 78.6%, with a domain-averaged value of 30.3%. Regionally, SNO_x contribute 5.5 μg m^{-3} (37.1%) and 2.5 μg m^{-3} (31.8%) to the surface NO_2 in the BTH and FWP regions, respectively, which are both higher than the domain-averaged

359 contribution. Although SHONO fluxes are lower than that of SNO_x in this period, its
360 effect on ambient HONO cannot be ignored. Over the study region, the contribution of
361 SHONO to surface HONO concentration ranges from 0 to 49.0%, with a domain-
362 averaged value of 35.6%. For the selected key regions, there are 1.8 $\mu g/m^3$ (36.7%) and
363 1.5 $\mu g/m^3$ (38.0%) of the monthly average HONO concentrations in the BTH and FWP
364 regions, respectively, from soil emissions. It is noteworthy that, despite the surface NO_2
365 (HONO) concentrations in the study regions being impacted by less than 13% (17%)
366 due to SHONO (SNO_x), the combined effects of soil Nr emissions on surface NO_2
367 (HONO) are found to be greater than the individual effects, which are 38.4% (40.3%)
368 for BTH and 33.9% (40.1%) for FWP region, respectively (Table S5). These results
369 highlight the importance of considering the cumulative impacts of multiple reactive
370 nitrogen emissions from soils on air pollution.

371 Consequently, substantial soil Nr emissions in July have a non-negligible effect on
372 atmospheric oxidation and the formation of secondary pollutants. For atmospheric
373 oxidation, we assess the impact of soil Nr emission on the maximum 1 h (max-1h) ·OH
374 levels and find that SHONO have a potential to increase the max-1h ·OH in most areas,
375 with a domain-averaged increase of 10.0%. On the contrary, the inclusion of SNO_x
376 results in a significant reduction of 31.3% in the max-1h ·OH across the entire study
377 domain. Considering the combined effect of SNO_x and SHONO, there is an overall
378 decrease of 24.3% in the max-1h ·OH over the study domain, with the BTH region
379 experiencing a decrease of 22.6% and FWP region showing a relatively greater
380 reduction of 32.2% (Table S6). These findings are different from the previous study,

which showed that soil background emissions including NO_x and HONO led to a 7.5% increase in max-1h ·OH in China (Wang et al., 2023c). The discrepancy between our findings and those of other studies regarding the impact of SNO_x on ·OH levels could be attributed to the abundance of ambient NH_3 in China during summer, where soil emissions may lead to a significant increase in nitrate, and the increased aerosols can affect the concentrations of ·OH through photochemical reactions (Wang et al., 2011; Xu et al., 2022). Additionally, after taking into account the SNO_x in the model, the environment may shift to a relatively NO_x-saturated regime, thus the termination reaction for O_3 production could be NO_2 and ·OH to generate HNO_3 (Chen et al., 2022; Wang et al., 2023b).We also stress the crucial role of SNO_x in influencing ·OH concentrations and highlight the varying impacts across different regions. For secondary pollutants, substantial O_3 enhancement is found in Henan and Hubei provinces, while the increase in nitrate is consistent with the spatial pattern of surface NO_2 from soil emissions. Specifically, soil Nr emissions increase the monthly average MDA8 O_3 and nitrate concentrations by 18.2% and 31.8%, respectively, across the study domain, with the increase of 16.9% and 42.4% in the BTH region and 17.2% and 42.7% in the FWP region. Moreover, SNO_x have a stronger effect on O_3 and nitrate in North China in July than those of SHONO.

The ratio of surface H_2O_2 to HNO_3 concentrations (hereafter H_2O_2/HNO_3) was used as an indicator of the O_3 formation regime to study the changes in sensitivity of summer O_3 to its precursors after considering the soil Nr emissions. The threshold of H_2O_2/HNO_3 for determining O_3 formation regime varies regionally (Sillman, 1995),

thus in this study, we identify the regions with H_2O_2/HNO_3 values greater than 0.65 as NO_x-sensitive regime, H_2O_2/HNO_3 values lower than 0.35 as VOCs-sensitive regime, and H_2O_2/HNO_3 values between 0.35 and 0.65 as VOCs-NO_x mixed sensitive regime (Shen et al., 2023). Figure 6 illustrates that the majority of BTH region has H_2O_2/HNO_3 values lower than 0.35 in Base simulation, indicating a VOCs-sensitive regime or NO_x-saturated regime in July. In contrast, the distribution of sensitivity of O_3 to precursor emission in FWP regions is more complex with a mix of three O_3 formation regimes. The spatial patterns of O_3 formation regimes presented in this study are consistent with the previous studies based on satellite observations and model simulations during summer seasons, despite using a different method (Wang et al., 2019; Wang et al., 2023b). This agreement across multiple approaches strengthens the confidence in the spatial patterns of O_3 formation regimes in the key regions of China. However, when soil nitrogen emissions are excluded, the H_2O_2/HNO_3 values mostly increase within 40% and the O_3 formation regime shifts to VOCs-NO_x mixed sensitive regime and NO_x-sensitive regime in both BTH and FWP regions. Although soil Nr emissions are lower than anthropogenic emissions, they still could affect the sensitivity of O_3 to its precursors and thus have an impact on the effectiveness of emission reduction policies. Therefore, soil emissions must be considered in formatting policies for the prevention and management of O_3 pollution.

3.3 Implication on O_3 mitigation strategies and temperature rise

Due to the influence of soil Nr emissions, the sensitivity of O_3 pollution to its precursors varies spatially, depending on the local levels of anthropogenic emissions. It

425 is thus important to quantify the role of soil Nr emissions in O_3 pollution regulation for
426 improving the effectiveness of air control measures. We conduct a series of sensitivity
427 experiments with anthropogenic NO_x emissions reduced by 20%, 40%, 60%, 80% and
428 100%, respectively, relative to the Base simulation (Table 1), and analyze the difference
429 in the response of surface O_3 concentrations to the anthropogenic NO_x emissions
430 reductions in the presence and absence of soil Nr emissions. Figure 7 shows that with
431 the reduction of anthropogenic NO_x emissions, MDA8 O_3 concentrations show an
432 accelerated decreasing trend, suggesting increasing efficiency of anthropogenic NO_x
433 control measures. And MDA8 O_3 response to anthropogenic NO_x emissions in the BTH
434 region is more curved (nonlinear) than that in the FWP region, which is consistent with
435 the fact that the BTH tends to have more NO_x-saturated regime (Figure 6).

436 It is noted that the reduction of anthropogenic NO_x emissions in the presence of
437 soil Nr emissions leads to a slower decrease in MDA8 O_3 compared to when soil Nr
438 emissions are excluded. We further analyze the details of the domain-averaged MDA8
439 O_3 changes under different anthropogenic reduction scenarios for the two key regions.
440 Specifically, in the BTH region, MDA8 O_3 decrease by 1.3% (1.8 μg m^{-3}), 6.3% (8.7
441 μg m^{-3}), and 17.4% (24.0 μg m^{-3}) with anthropogenic NO_x emission reductions by 20%,
442 60%, and 100%, respectively, in the present of soil Nr emissions. Comparatively, in the
443 absence of soil Nr emissions, the reductions in MDA8 O_3 are more pronounced and
444 decrease by 2.3% (2.7 μg m^{-3}), 10.7% (12.8 μg m^{-3}), and 42.3% (50.6 μg m^{-3}),
445 respectively. In the FWP region, with a 20% reduction in anthropogenic NO_x emissions,
446 MDA8 O_3 levels only exhibit a slight decrease of 1.7% (2.3 μg m^{-3}) in the presence of

447 soil Nr emissions, whereas a decrease of 2.3% (2.6 μg m^{-3}) is found in the absence of
448 soil Nr emissions. When anthropogenic NO_x emissions are removed entirely, MDA8
449 O_3 decreases by 13.6% (17.7 μg m^{-3}) in the presence of soil Nr emissions, and more
450 significant decreases are found in the absent of soil Nr emissions with a reduction of
451 27.4% (34.0 μg m^{-3}) (as shown in Figure 7b-c, e-f). We conclude that the existence of
452 soil Nr emissions could contribute to an additional part of O_3 production, amounting to
453 a range of 0-24.9% in the BTH and 0-13.8% in the FWP region in July, and these
454 suppressions could be enlarged over the rural areas where have more substantial soil Nr
455 emissions, i.e., 0-32.3% in cropland over the BTH and 0-15.0% in croplands over the
456 FWP region. These findings suggest that soil Nr emissions have the potential to
457 suppress the effectiveness of measures implemented to mitigate O_3 pollution, and this
458 effect becomes more significant as anthropogenic NO_x emissions decrease.

459 We also quantify the O_3 generated from soil Nr emission source (denoted as the
460 soil O_3) in July under the different anthropogenic NO_x emission reduction scenarios.
461 Overall, soil O_3 concentrations in croplands are higher than in non-croplands.
462 Regionally, in the BTH region, the soil O_3 concentrations are 19.8 μg m^{-3} under high
463 anthropogenic emissions level (referred to as the Base simulation), while the soil O_3
464 concentrations significantly increase to 46.4 μg m^{-3} when all anthropogenic NO_x
465 emissions are cut down (shown as red bar in Figure 7b). A similar trend is also found
466 in the FWP region, although soil Nr emissions are relatively lower than that in the BTH
467 region, the soil O_3 concentrations are 19.0 μg m^{-3} in the Base simulation, and do not
468 change significantly with the reduction of anthropogenic emissions, but increase to 31.9

469 μg m^{-3} when anthropogenic NO_x emissions are excluded (shown as red bar in Figure
470 7c). The reduction in anthropogenic NO_x emissions results in a shift of the O_3 formation
471 regime towards a more NO_x-sensitive regime, leading to a higher contribution of O_3
472 from soil emission sources. We conclude that with stricter anthropogenic emission
473 reduction measures, the contributions of soil Nr emissions to O_3 production in both
474 absolute and relative value would increase and further hamper the effectiveness of
475 anthropogenic emission reductions. To effectively mitigate O_3 pollutions, it is necessary
476 to implement much stricter control measures for anthropogenic emissions including
477 coal burning and transportation due to the synergistic effects of SNO_x and SHONO.
478 Here we show that the substantial soil Nr emissions present an additional challenge
479 for O_3 pollution regulation in the North China. We further assess the impact of soil Nr
480 emissions on air temperature change under different anthropogenic emission reduction
481 scenarios. Under the background of climate change, future emission reduction scenarios
482 should focus on the co-control of multiple air pollutants and greenhouse gas reductions.
483 Therefore, we conduct multi-pollutant co-control reduction scenarios, taking into
484 account the SO_2, NO_x, primary $PM_{2.5}$, VOCs, and CO emissions reduced by 20%, 40%,
485 60%, 80%, and 100%, respectively, to investigate the impact of soil Nr emissions on
486 air temperature change under different anthropogenic reduction scenarios (Table 1). By
487 comparing changes in air temperature at 2m (T2) with and without soil Nr emissions
488 under different reduction scenarios, Figure 8 shows that incorporating soil Nr emissions
489 results in a slower rate of T2 increase compared to scenarios without soil Nr emissions,
490 especially when multi-pollutant emissions are reduced to more than a half, and this

phenomenon is consistent across all study regions. In the FWP region, when anthropogenic emissions are eliminated, T2 increases by 0.073 ℃ in the presence of soil Nr emissions, compared to 0.095 ℃ in the absence of soil Nr emissions. In the BTH region, which has relatively high anthropogenic emissions, reducing multi-pollutant emissions by the same proportion could result in relatively greater warming, and T2 increases by 0.098 ℃ in the presence of soil Nr emissions, compared to 0.14 ℃ in the absence of soil Nr emissions when anthropogenic emissions are excluded. This is attributed to the effective radiative forcing (ERF) associated with the cooling effects of primary pollutants (e.g. SO_2, NO_x) and secondary inorganic aerosols (SIA), and positive ERF associated with the warming effects of CO and VOCs (high confidence) (Bellouin et al., 2020; Liao and Xie, 2021). Decreases in primary pollutants emissions and SIA concentrations could weaken the cooling effect and potentially accelerate warming to some extent, and the decrease in CO and VOCs emissions may still lead to temperature rise in a short-term. However, the soil Nr emissions could contribute to a certain background concentration of aerosol, partially offsetting the temperature rise caused by declining anthropogenic emissions of primary pollutants and greenhouse gas (Figure S8). Therefore, although soil Nr emissions are relatively low compared to anthropogenic emissions, the combined effects of NO_x and HONO emissions from natural soil and agricultural land should be considered when assessing climate change and implementing strategies to mitigate O_3 pollution.

4. Conclusions

In this study, the updated soil Nr emission scheme was implemented in the UI-

513 WRF-Chem model and used to estimate the combined and individual impact of SNO_x
514 and SHONO on subsequent changes in air quality and air temperature rise in North
515 China, with a focus on two key regions (the BTH and FWP regions) because of high
516 levels of soil Nr and anthropogenic emissions. We show that the SNO_x fluxes are almost
517 twice as high as SHONO during July 2018, with higher soil emissions in areas with
518 extensive cropland. The contribution of soil Nr emissions in July to monthly average
519 NO_2 and HONO are 38.4% and 40.3% in the BTH, and 33.9% and 40.1% in the FWP
520 region, respectively, and the substantial soil Nr emissions lead to a considerable
521 increase in the monthly average MDA8 O_3 and nitrate concentrations, with the values
522 of 16.9% and 42.4% in the BTH region and 17.2% and 42.7% in the FWP region, which
523 both exceed the individual SNO_x or SHONO effect. The presence of soil Nr emissions,
524 acting as precursors of O_3 and SIA, has a suppressing effect on efforts to mitigate
525 summer O_3 pollution, particularly in the BTH region, and also leads to a slower increase
526 rate of T2 (0.098 ℃) in July compared to scenarios without soil Nr emissions (0.14 ℃)
527 when anthropogenic emissions are excluded. We note that the effect of soil Nr emissions
528 shows spatial heterogeneity under different anthropogenic emissions reduction
529 scenarios.

530 However, we admit that uncertainties exist in both soil Nr and anthropogenic
531 emissions, as well as the parameterization scheme of HONO sources. The agricultural
532 emissions of another important reactive nitrogen gas, NH_3, may also be underestimated
533 due to uncertainties in agricultural fertilizer application and livestock waste in MEIC
534 inventory (Li et al., 2021a). These uncertainties could impact the aerosol formation and

local cooling effect. Also, the discrepancies between simulated and observed NO_2, O_3, and other air pollutants in the model may affect the assessment of the role of soil Nr emissions in O_3 mitigation strategies and their impact on climate change. Thus, more direct measurements of soil Nr fluxes are crucial to better constrain soil emissions and improve the parametrization in the model.

Our study highlights that despite soil Nr emissions being lower than anthropogenic emissions, they still have a substantial impact on the effectiveness of O_3 pollution mitigation measures, and this effect becomes more significant as anthropogenic emissions decrease. Therefore, reactive nitrogen from soil emission sources must be considered in formatting measures for the prevention and management of O_3 pollution, as well as addressing climate change.

Code and data availability. Some of the data repositories have been listed in Section 2. The other data, model outputs and codes can be accessed by contacting Tong Sha via tong-sha@sust.edu.cn.

Author contributions. TS performed the model simulation, data analysis and manuscript writing. TS and JW proposed the idea. SY, QC and LL supervised this work and revised the manuscript. XM, ZF and KB helped the revision of the manuscript. YZ provided and analyzed the observation data.

Competing interests. The authors declare that they have no conflict of interest.

Acknowledgements. This study is supported by the National Natural Science Foundation of China (grant nos. 42205107, 42130714). Jun Wang's participation is made possible via the in-kind support from the University of Iowa.

References

Akimoto, H., Nagashima, T., Li, J., Fu, J. S., Ji, D., Tan, J., and Wang, Z.: Comparison of surface ozone simulation among selected regional models in MICS-Asia III – effects of chemistry and vertical transport for the causes of difference, Atmos. Chem. Phys., 19, 603-615, 10.5194/acp-19-603-2019, 2019.

Almaraz, M., Bai, E., Wang, C., Trousdell, J., Conley, S., Faloona, I., and Houlton, B. Z.: Agriculture is a major source of NO_x pollution in California, Sci. Adv., 4(1), eaao3477., 2018.

Bellouin, N., Quaas, J., Gryspeerdt, E., Kinne, S., Stier, P., Watson-Parris, D., Boucher, O., Carslaw, K. S., Christensen, M., and Daniau, A. L.: Bounding global aerosol radiative forcing of climate change, Rev. Geophys., 58, e2019RG000660, 2020.

Chen, K., Wang, P., Zhao, H., Wang, P., Gao, A., Myllyvirta, L., and Zhang, H.: Summertime O_3 and related health risks in the north China plain: A modeling study using two anthropogenic emission inventories, Atmos. Environ., 246, 118087,

10.1016/j.atmosenv.2020.118087, 2021.

Chen, W., Guenther, A. B., Jia, S., Mao, J., Yan, F., Wang, X., and Shao, M.: Synergistic effects of biogenic volatile organic compounds and soil nitric oxide emissions on summertime ozone formation in China, Sci. Total Environ., 828, 154218, 10.1016/j.scitotenv.2022.154218, 2022.

Elshorbany, Y. F., Steil, B., Brühl, C., and Lelieveld, J.: Impact of HONO on global atmospheric chemistry calculated with an empirical parameterization in the EMAC model, Atmos. Chem. Phys., 12, 9977-10000, 10.5194/acp-12-9977-2012, 2012.

Feng, T., Zhao, S., Liu, L., Long, X., Gao, C., and Wu, N.: Nitrous acid emission from soil bacteria and related environmental effect over the North China Plain, Chemosphere, 287, 132034, 10.1016/j.chemosphere.2021.132034, 2022a.

Feng, Z., Xu, Y., Kobayashi, K., Dai, L., Zhang, T., Agathokleous, E., Calatayud, V., Paoletti, E., Mukherjee, A., Agrawal, M., Park, R. J., Oak, Y. J., and Yue, X.: Ozone pollution threatens the production of major staple crops in East Asia, Nat. Food, 3, 47-56, 10.1038/s43016-021-00422-6, 2022b.

Fu, X., Wang, T., Zhang, L., Li, Q., Wang, Z., Xia, M., Yun, H., Wang, W., Yu, C., Yue, D., Zhou, Y., Zheng, J., and Han, R.: The significant contribution of HONO to secondary pollutants during a severe winter pollution event in southern China, Atmos. Chem. Phys., 19, 1-14, 10.5194/acp-19-1-2019, 2019.

Gelaro, R., McCarty, W., Suárez, M. J., Todling, R., Molod, A., Takacs, L., Randles, C. A., Darmenov, A., Bosilovich, M. G., Reichle, R., Wargan, K., Coy, L., Cullather, R., Draper, C., Akella, S., Buchard, V., Conaty, A., da Silva, A. M., Gu, W., Kim, G.-K., Koster, R., Lucchesi, R., Merkova, D., Nielsen, J. E., Partyka, G., Pawson, S., Putman, W., Rienecker, M., Schubert, S. D., Sienkiewicz, M., and Zhao, B.: The Modern-Era Retrospective Analysis for Research and Applications, Version 2 (MERRA-2), J. Clim., 30, 5419-5454, 10.1175/jcli-d-16-0758.1, 2017.

Grell, G. A. and Dévényi, D.: A generalized approach to parameterizing convection combining ensemble and data assimilation techniques, Geophys. Res. Lett., 29, 10.1029/2002gl015311, 2002.

Grell, G. A., Peckham, S. E., Schmitz, R., McKeen, S. A., Frost, G., Skamarock, W. C., and Eder, B.: Fully coupled “online” chemistry within the WRF model, Atmos. Environ., 39, 6957-6975, 10.1016/j.atmosenv.2005.04.027, 2005.

Guenther, A. B., Jiang, X., Heald, C. L., Sakulyanontvittaya, T., Duhl, T., Emmons, L. K., and Wang, X.: The Model of Emissions of Gases and Aerosols from Nature version 2.1 (MEGAN2.1): an extended and updated framework for modeling biogenic emissions, Geosci. Model Dev., 5, 1471-1492, 10.5194/gmd-5-1471-2012, 2012.

Hong, S. Y., Noh, Y., and Dudhia, J.: A new vertical diffusion package with an explicit treatment of entrainment processes, Mon. Weather Rev., 134 (9), 2318, 10.1175/MWR3199.1, 2006.

Huang, L., Fang, J., Liao, J., Yarwood, G., Chen, H., Wang, Y., and Li, L.: Insights into soil NO emissions and the contribution to surface ozone formation in China, Atmos. Chem. Phys., 23, 14919-14932, 10.5194/acp-23-14919-2023, 2023.

Huang, Y., Hickman, J. E., and Wu, S.: Impacts of enhanced fertilizer applications on tropospheric ozone and crop damage over sub-Saharan Africa, Atmos. Environ., 180, 117-125, 10.1016/j.atmosenv.2018.02.040, 2018.

Huber, D. E., Steiner, A. L., and Kort, E. A.: Sensitivity of Modeled Soil NO_x Emissions to Soil Moisture, J. Geophys. Res.: Atmos., 128, 10.1029/2022jd037611, 2023.

Iacono, M. J., Delamere, J. S., Mlawer, E. J., Shephard, M. W., Clough, S. A., and Collins, W. D.: Radiative forcing by long-lived greenhouse gases: Calculations with the AER radiative transfer models, J. Geophys. Res.: Atmos., 113, 10.1029/2008jd009944, 2008.

Li, B., Chen, L., Shen, W., Jin, J., Wang, T., Wang, P., Yang, Y., and Liao, H.: Improved gridded ammonia emission inventory in China, Atmos. Chem. Phys., 21, 15883-15900, 10.5194/acp-21-15883-2021, 2021a.

Li, C., Wang, J., Zhang, H., Diner, D. J., Hasheminassab, S., and Janechek, N.: Improvement of Surface $PM_{2.5}$ Diurnal Variation Simulations in East Africa for the MAIA Satellite Mission, ACS ES&T Air, 10.1021/acsestair.3c00008, 2024.

Li, G., Lei, W., Zavala, M., Volkamer, R., Dusanter, S., Stevens, P., and Molina, L. T.:

633 Impacts of HONO sources on the photochemistry in Mexico City during the
634 MCMA-2006/MILAGO Campaign, Atmos. Chem. Phys., 10, 6551-6567,
635 10.5194/acp-10-6551-2010, 2010.
636 Li, K., Jacob, D. J., Shen, L., Lu, X., De Smedt, I., and Liao, H.: Increases in surface
637 ozone pollution in China from 2013 to 2019: anthropogenic and meteorological
638 influences, Atmos. Chem. Phys., 20, 11423-11433, 10.5194/acp-20-11423-2020,
639 2020.
640 Li, K., Jacob, D. J., Liao, H., Zhu, J., Shah, V., Shen, L., Bates, K. H., Zhang, Q., and
641 Zhai, S.: A two-pollutant strategy for improving ozone and particulate air quality
642 in China, Nat. Geosci., 12, 906-910, 10.1038/s41561-019-0464-x, 2019.
643 Li, K., Jacob, D. J., Liao, H., Qiu, Y., Shen, L., Zhai, S., Bates, K. H., Sulprizio, M. P.,
644 Song, S., Lu, X., Zhang, Q., Zheng, B., Zhang, Y., Zhang, J., Lee, H. C., and Kuk,
645 S. K.: Ozone pollution in the North China Plain spreading into the late-winter haze
646 season, Proc. Natl. Acad. Sci. U.S.A., 118, 10.1073/pnas.2015797118, 2021b.
647 Liao, H. and Xie, P.: The roles of short-lived climate forcers in a changing climate, Adv.
648 Clim. Change Res., 17, 685, 2021.
649 Liu, X., Zhang, Y., Han, W., Tang, A., Shen, J., Cui, Z., Vitousek, P., Erisman, J. W.,
650 Goulding, K., Christie, P., Fangmeier, A., and Zhang, F.: Enhanced nitrogen
651 deposition over China, Nature, 494, 459-462, 10.1038/nature11917, 2013.
652 Liu, Y. and Wang, T.: Worsening urban ozone pollution in China from 2013 to 2017 –
653 Part 1: The complex and varying roles of meteorology, Atmos. Chem. Phys., 20,
654 6305-6321, 10.5194/acp-20-6305-2020, 2020a.
655 Liu, Y. and Wang, T.: Worsening urban ozone pollution in China from 2013 to 2017 –
656 Part 2: The effects of emission changes and implications for multi-pollutant
657 control, Atmos. Chem. Phys., 20, 6323-6337, 10.5194/acp-20-6323-2020, 2020b.
658 Lu, C. and Tian, H.: Global nitrogen and phosphorus fertilizer use for agriculture
659 production in the past half century: shifted hot spots and nutrient imbalance, Earth
660 Syst. Sci. Data, 9, 181-192, 10.5194/essd-9-181-2017, 2017.
661 Lu, X., Zhang, L., Chen, Y., Zhou, M., Zheng, B., Li, K., Liu, Y., Lin, J., Fu, T.-M., and
662 Zhang, Q.: Exploring 2016–2017 surface ozone pollution over China: source

contributions and meteorological influences, Atmos. Chem. Phys., 19, 8339-8361, 10.5194/acp-19-8339-2019, 2019.

Lu, X., Ye, X., Zhou, M., Zhao, Y., Weng, H., Kong, H., Li, K., Gao, M., Zheng, B., Lin, J., Zhou, F., Zhang, Q., Wu, D., Zhang, L., and Zhang, Y.: The underappreciated role of agricultural soil nitrogen oxide emissions in ozone pollution regulation in North China, Nat. Commun., 12, 10.1038/s41467-021-25147-9, 2021.

Morrison, H., Thompson, G., and Tatarskii, V.: Impact of Cloud Microphysics on the Development of Trailing Stratiform Precipitation in a Simulated Squall Line: Comparison of One- and Two-Moment Schemes, Mon. Weather Rev., 137, 991-1007, 10.1175/2008mwr2556.1, 2009.

Oswald, R., Behrendt, T., Ermel, M., Wu, D., Su, H., Cheng, Y., Breuninger, C., Moravek, A., Mougin, E., Delon, C., Loubet, B., Pommerening-Röser, A., Sörgel, M., Pöschl, U., Hoffmann, T., Andreae, M. O., Meixner, F. X., and Trebs, I.: HONO Emissions from Soil Bacteria as a Major Source of Atmospheric Reactive Nitrogen, Science, 341, 1233-1235, 10.1126/science.1242266, 2013.

Pinder, R. W., Davidson, E. A., Goodale, C. L., Greaver, T. L., Herrick, J. D., and Liu, L.: Climate change impacts of US reactive nitrogen, Proc. Natl. Acad. Sci. U.S.A., 109, 7671-7675, 10.1073/pnas.1114243109, 2012.

Reay, D. S., Dentener, F., Smith, P., Grace, J., and Feely, R. A.: Global nitrogen deposition and carbon sinks., Nat. Geosci., 1(7), 430-437, 10.1038/ngeo230, 2008.

Rodell, M., Houser, P. R., Jambor, U., Gottschalck, J., Mitchell, K., Meng, C.-J., Arsenault, K., Cosgrove, B., Radakovich, J., Bosolovich, M., Entin, J. K., Walker, J. P., Lohmann, D., and Toll, D.: The global land data assimilation system, Bull. Am. Meteorol. Soc., 85, 381–394, 10.1175/BAMS-85-3-381, 2004.

Romer, P. S., Duffey, K. C., Wooldridge, P. J., Edgerton, E., Baumann, K., Feiner, P. A., Miller, D. O., Brune, W. H., Koss, A. R., de Gouw, J. A., Misztal, P. K., Goldstein, A. H., and Cohen, R. C.: Effects of temperature-dependent NO_x emissions on continental ozone production, Atmos. Chem. Phys., 18, 2601-2614, 10.5194/acp-18-2601-2018, 2018.

Sha, T., Ma, X., Zhang, H., Janechek, N., Wang, Y., Wang, Y., Castro García, L., Jenerette, G. D., and Wang, J.: Impacts of Soil NO_x Emission on O_3 Air Quality in Rural California, Environ. Sci. Technol., 55, 7113-7122, 10.1021/acs.est.0c06834, 2021.

Shen, Y., Xiao, Z., Wang, Y., Xiao, W., Yao, L., and Zhou, C.: Impacts of Agricultural Soil NO_x Emissions on O_3 Over Mainland China, J. Geophys. Res.: Atmos., 128, 10.1029/2022jd037986, 2023.

Sillman, S.: The use of NO_y, H_2O_2, and HNO_3 as indicators for ozone-NO_x-hydrocarbon sensitivity in urban locations, J. Geophys. Res., 100(D7), 14175–14188., 10.1029/94JD02953, 1995.

Skiba, U., Medinets, S., Cardenas, L. M., Carnell, E. J., Hutchings, N., and Amon, B.: Assessing the contribution of soil NO_x emissions to European atmospheric pollution, Environ. Res. Lett., 10.1088/1748-9326/abd2f2, 2020.

Sun, L., Xue, L., Wang, Y., Li, L., Lin, J., Ni, R., Yan, Y., Chen, L., Li, J., Zhang, Q., and Wang, W.: Impacts of meteorology and emissions on summertime surface ozone increases over central eastern China between 2003 and 2015, Atmos. Chem. Phys., 19, 1455-1469, 10.5194/acp-19-1455-2019, 2019.

Tan, W., Wang, H., Su, J., Sun, R., He, C., Lu, X., Lin, J., Xue, C., Wang, H., Liu, Y., Liu, L., Zhang, L., Wu, D., Mu, Y., and Fan, S.: Soil Emissions of Reactive Nitrogen Accelerate Summertime Surface Ozone Increases in the North China Plain, Environ. Sci. Technol., 57, 12782-12793, 10.1021/acs.est.3c01823, 2023.

Tewari, M., Chen, F., Wang, W., Dudhia, J., LeMone, M. A., Mitchell, K., Ek, M., Gayno, G., Wegiel, J., and Cuenca, R. H.: Implementation and verification of the unified NOAH land surface model in the WRF model, 20th Conference on Weather Analysis and Forecasting/16th Conference on Numerical Weather Prediction, 11–15., 2004.

Travis, K. R. and Jacob, D. J.: Systematic bias in evaluating chemical transport models with maximum daily 8 h average (MDA8) surface ozone for air quality applications: a case study with GEOS-Chem v9.02, Geosci. Model Dev., 12, 3641-3648, 10.5194/gmd-12-3641-2019, 2019.

723 Turner, M. C., Jerrett, M., Pope, C. A., Krewski, D., Gapstur, S. M., Diver, W. R.,
724 Beckerman, B. S., Marshall, J. D., Su, J., Crouse, D. L., and Burnett, R. T.: Long-
725 Term Ozone Exposure and Mortality in a Large Prospective Study, Am. J. Resp.
726 Crit. Care., 193, 1134-1142, 10.1164/rccm.201508-1633OC, 2016.
727 Unger, N., Zheng, Y., Yue, X., and Harper, K. L.: Mitigation of ozone damage to the
728 world's land ecosystems by source sector, Nat. Clim. Change, 10, 134-137,
729 10.1038/s41558-019-0678-3, 2020.
730 van Geffen, J., Boersma, K. F., Eskes, H., Sneep, M., ter Linden, M., Zara, M., and
731 Veefkind, J. P.: S5P TROPOMI NO_2 slant column retrieval: method, stability,
732 uncertainties and comparisons with OMI, Atmos. Meas. Tech., 13, 1315-1335,
733 10.5194/amt-13-1315-2020, 2020.
734 van Geffen, J. H. G. M., Eskes, H. J., Boersma, K. F., and Veefkind, J. P.: TROPOMI
735 ATBD of the total and tropospheric NO_2 data products, Report S5P-KNMI-L2-
736 0005-RP, version 2.2.0, 2021-06-16, KNMI, De Bilt, The Netherlands,
737 http://www.tropomi.eu/data-products/nitrogen-dioxide/ (last access: 7 March
738 2022), 2021.
739 Vinken, G. C. M., Boersma, K. F., Maasakkers, J. D., Adon, M., and Martin, R. V.:
740 Worldwide biogenic soil NO_x emissions inferred from OMI NO_2 observations,
741 Atmos. Chem. Phys., 14, 10363-10381, 10.5194/acp-14-10363-2014, 2014.
742 Wang, N., Lyu, X., Deng, X., Huang, X., Jiang, F., and Ding, A.: Aggravating O_3
743 pollution due to NO_x emission control in eastern China, Sci. Total Environ., 677,
744 732-744, 10.1016/j.scitotenv.2019.04.388, 2019.
745 Wang, Q. g., Han, Z., Wang, T., and Zhang, R.: Impacts of biogenic emissions of VOC
746 and NO_x on tropospheric ozone during summertime in eastern China, Sci. Total
747 Environ., 395, 41-49, 10.1016/j.scitotenv.2008.01.059, 2008.
748 Wang, R., Bei, N., Wu, J., Li, X., Liu, S., Yu, J., Jiang, Q., Tie, X., and Li, G.: Cropland
749 nitrogen dioxide emissions and effects on the ozone pollution in the North China
750 plain, Environ. Pollut., 294, 118617, 10.1016/j.envpol.2021.118617, 2022a.
751 Wang, R., Bei, N., Pan, Y., Wu, J., Liu, S., Li, X., Yu, J., Jiang, Q., Tie, X., and Li, G.:
752 Urgency of controlling agricultural nitrogen sources to alleviate summertime air

753 pollution in the North China Plain, Chemosphere, 311, 137124,
754 10.1016/j.chemosphere.2022.137124, 2023a.
755 Wang, S., Xing, J., Jang, C., Zhu, Y., Fu, J. S., and Hao, J.: Impact Assessment of
756 Ammonia Emissions on Inorganic Aerosols in East China Using Response Surface
757 Modeling Technique, Environ. Sci. Technol., 45, 9293-9300, 10.1021/es2022347,
758 2011.
759 Wang, W., Parrish, D. D., Wang, S., Bao, F., Ni, R., Li, X., Yang, S., Wang, H., Cheng,
760 Y., and Su, H.: Long-term trend of ozone pollution in China during 2014–2020:
761 distinct seasonal and spatial characteristics and ozone sensitivity, Atmos. Chem.
762 Phys., 22, 8935-8949, 10.5194/acp-22-8935-2022, 2022b.
763 Wang, W., Li, X., Cheng, Y., Parrish, D. D., Ni, R., Tan, Z., Liu, Y., Lu, S., Wu, Y., Chen,
764 S., Lu, K., Hu, M., Zeng, L., Shao, M., Huang, C., Tian, X., Leung, K. M., Chen,
765 L., Fan, M., Zhang, Q., Rohrer, F., Wahner, A., Pöschl, U., Su, H., and Zhang, Y.:
766 Ozone pollution mitigation strategy informed by long-term trends of atmospheric
767 oxidation capacity, Nat. Geosci., 17, 20-25, 10.1038/s41561-023-01334-9, 2023b.
768 Wang, Y., Ge, C., Castro Garcia, L., Jenerette, G. D., Oikawa, P. Y., and Wang, J.:
769 Improved modelling of soil NO_x emissions in a high temperature agricultural
770 region: role of background emissions on NO_2 trend over the US, Environ. Res.
771 Lett., 16, 084061, 10.1088/1748-9326/ac16a3, 2021a.
772 Wang, Y., Fu, X., Wang, T., Ma, J., Gao, H., Wang, X., and Pu, W.: Large Contribution
773 of Nitrous Acid to Soil-Emitted Reactive Oxidized Nitrogen and Its Effect on Air
774 Quality, Environ. Sci. Technol., 57, 3516-3526, 10.1021/acs.est.2c07793, 2023c.
775 Wang, Y., Fu, X., Wu, D., Wang, M., Lu, K., Mu, Y., Liu, Z., Zhang, Y., and Wang, T.:
776 Agricultural Fertilization Aggravates Air Pollution by Stimulating Soil Nitrous
777 Acid Emissions at High Soil Moisture, Environ. Sci. Technol., 55, 14556-14566,
778 10.1021/acs.est.1c04134, 2021b.
779 Wang, Y., Wang, J., Zhang, H., Janechek, N., Wang, Y., Zhou, M., Shen, P., Tan, J., He,
780 Q., Cheng, T., and Huang, C.: Impact of land use change on the urban-rural
781 temperature disparity in Eastern China, Atmos. Environ., 308, 119850,
782 10.1016/j.atmosenv.2023.119850, 2023d.

Weber B, W. D., Tamm A, et al. : Biological soil crusts accelerate the nitrogen cycle through large NO and HONO emissions in drylands, Proc. Natl. Acad. Sci. U.S.A., 112(50): 15384-15389., 2015.

Wei, J., Li, Z., Li, K., Dickerson, R. R., Pinker, R. T., Wang, J., Liu, X., Sun, L., Xue, W., and Cribb, M.: Full-coverage mapping and spatiotemporal variations of ground-level ozone (O_3) pollution from 2013 to 2020 across China, Remote Sens. Environ., 270, 112775, 10.1016/j.rse.2021.112775, 2022.

Xu, W., Kuang, Y., Zhao, C., Tao, J., Zhao, G., Bian, Y., Yang, W., Yu, Y., Shen, C., Liang, L., Zhang, G., Lin, W., and Xu, X.: NH_3-promoted hydrolysis of NO_2 induces explosive growth in HONO, Atmos. Chem. Phys., 19, 10557-10570, 10.5194/acp-19-10557-2019, 2019.

Xu, W., Zhao, Y., Wen, Z., Chang, Y., Pan, Y., Sun, Y., Ma, X., Sha, Z., Li, Z., Kang, J., Liu, L., Tang, A., Wang, K., Zhang, Y., Guo, Y., Zhang, L., Sheng, L., Zhang, X., Gu, B., Song, Y., Van Damme, M., Clarisse, L., Coheur, P.-F., Collett, J. L., Goulding, K., Zhang, F., He, K., and Liu, X.: Increasing importance of ammonia emission abatement in $PM_{2.5}$ pollution control, Sci. Bull., 67, 1745-1749, 10.1016/j.scib.2022.07.021, 2022.

Yan, X., Ohara, T., and Akimoto, H.: Statistical modeling of global soil NO_x emissions, Global Biogeochem. Cycles, 19, 10.1029/2004gb002276, 2005.

Yang, J. and Zhao, Y.: Performance and application of air quality models on ozone simulation in China – A review, Atmos. Environ., 293, 119446, 10.1016/j.atmosenv.2022.119446, 2023.

Ye, C., Gao, H., Zhang, N., and Zhou, X.: Photolysis of Nitric Acid and Nitrate on Natural and Artificial Surfaces, Environ. Sci. Technol., 50, 3530-3536, 10.1021/acs.est.5b05032, 2016.

Ye, C., Zhang, N., Gao, H., and Zhou, X.: Photolysis of Particulate Nitrate as a Source of HONO and NO_x, Environ. Sci. Technol., 51, 6849-6856, 10.1021/acs.est.7b00387, 2017.

Ye, X., Wang, X., and Zhang, L.: Diagnosing the Model Bias in Simulating Daily Surface Ozone Variability Using a Machine Learning Method: The Effects of Dry

Deposition and Cloud Optical Depth, Environ. Sci. Technol., 56, 16665-16675, 10.1021/acs.est.2c05712, 2022.

Yue, X., Unger, N., Harper, K., Xia, X., Liao, H., Zhu, T., Xiao, J., Feng, Z., and Li, J.: Ozone and haze pollution weakens net primary productivity in China, Atmos. Chem. Phys., 17, 6073-6089, 10.5194/acp-17-6073-2017, 2017.

Zaveri, R. A. and Peters, L. K.: A new lumped structure photochemical mechanism for large-scale applications, J. Geophys. Res.: Atmos., 104, 30387-30415, 10.1029/1999jd900876, 1999.

Zaveri, R. A., Easter, R. C., Fast, J. D., and Peters, L. K.: Model for Simulating Aerosol Interactions and Chemistry (MOSAIC), J. Geophys. Res.: Atmos., 113, 10.1029/2007jd008782, 2008.

Zhan, Y., Xie, M., Gao, D., Wang, T., Zhang, M., and An, F.: Characterization and source analysis of water-soluble inorganic ionic species in $PM_{2.5}$ during a wintertime particle pollution episode in Nanjing, China, Atmos. Res., 262, 105769, 10.1016/j.atmosres.2021.105769, 2021.

Zhang, J., Ran, H., Guo, Y., Xue, C., Liu, X., Qu, Y., Sun, Y., Zhang, Q., Mu, Y., Chen, Y., Wang, J., and An, J.: High crop yield losses induced by potential HONO sources — A modelling study in the North China Plain, Sci. Total Environ., 803, 149929, 10.1016/j.scitotenv.2021.149929, 2022a.

Zhang, J., Lian, C., Wang, W., Ge, M., Guo, Y., Ran, H., Zhang, Y., Zheng, F., Fan, X., Yan, C., Daellenbach, K. R., Liu, Y., Kulmala, M., and An, J.: Amplified role of potential HONO sources in O_3 formation in North China Plain during autumn haze aggravating processes, Atmos. Chem. Phys., 22, 3275-3302, 10.5194/acp-22-3275-2022, 2022b.

Zhang, L., Wang, T., Zhang, Q., Zheng, J., Xu, Z., and Lv, M.: Potential sources of nitrous acid (HONO) and their impacts on ozone: A WRF-Chem study in a polluted subtropical region, J. Geophys. Res.: Atmos., 121, 3645-3662, 10.1002/2015jd024468, 2016.

Zhang, S., Sarwar, G., Xing, J., Chu, B., Xue, C., Sarav, A., Ding, D., Zheng, H., Mu, Y., Duan, F., Ma, T., and He, H.: Improving the representation of HONO chemistry

in CMAQ and examining its impact on haze over China, Atmos. Chem. Phys., 21, 15809-15826, 10.5194/acp-21-15809-2021, 2021.

Zhang, W., Tong, S., Jia, C., Wang, L., Liu, B., Tang, G., Ji, D., Hu, B., Liu, Z., Li, W., Wang, Z., Liu, Y., Wang, Y., and Ge, M.: Different HONO Sources for Three Layers at the Urban Area of Beijing, Environ. Sci. Technol., 54, 12870-12880, 10.1021/acs.est.0c02146, 2020.

Table 1. Description of model simulation experiments.

Simulation	Soil emissions		Anthropogenic emissions		
	Soil NO_x	Soil HONO	NO_x	VOCs	Others
Default	1(MEGAN)	0	1	1	1
Base	1(BDISNP)	1	1	1	1
NoSoilNr	0	0	1	1	1
NoSHONO	1	0	1	1	1
NoSNO_x	0	1	1	1	1
Base_redANO_x	1	1	0.8/0.6/0.4/0.2/0[a]	1	1
NoSoil_redANO_x	0	0	0.8/0.6/0.4/0.2/0[b]	1	1
Base_redAnt	1	1	0.8/0.6/0.4/0.2/0[c]	0.8/0.6/0.4/0.2/0[d]	0.8/0.6/0.4/0.2/0[e]
NoSoil_redAnt	0	0	0.8/0.6/0.4/0.2/0[f]	0.8/0.6/0.4/0.2/0[g]	0.8/0.6/0.4/0.2/0[h]

[a-h] The values represent the reduction ratios applied to the anthropogenic emissions in the sensitivity simulations compared to the Base.

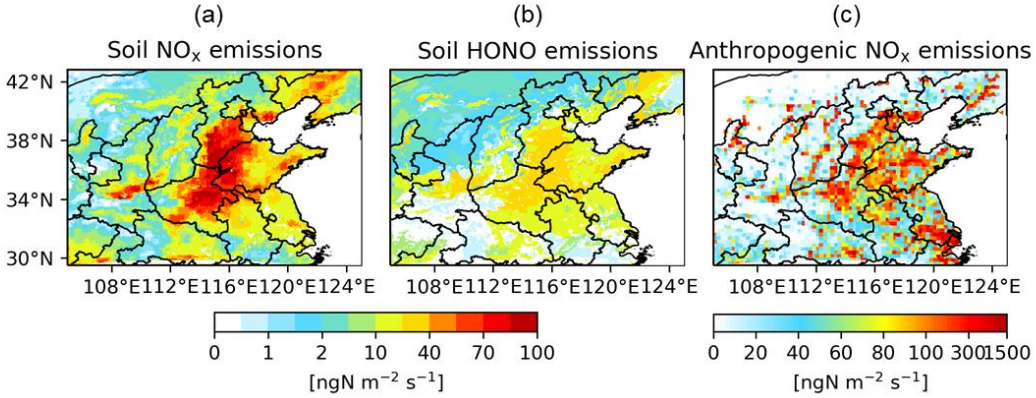

854

855 **Figure 1.** Distribution of the simulated monthly mean (a) soil NO_x emissions, (b) soil

856 HONO emissions, and (c) anthropogenic NO_x emissions in North China in July 2018.

857

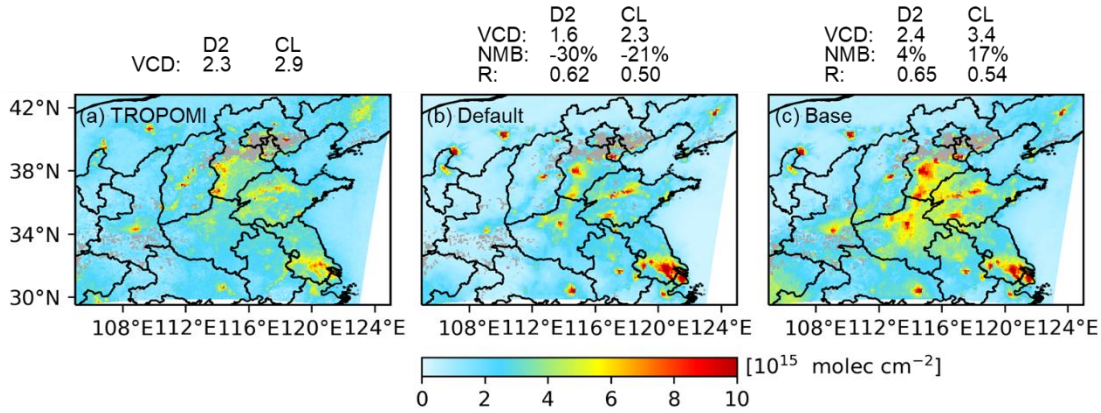

858

859 **Figure 2.** (a) Monthly mean tropospheric NO_2 VCD retrieved by TROPOMI measured

860 at 12:00−14:00 LT and simulated by (b) Default and (c) Base averaged over the same

861 periods in July 2018 in North China.

862

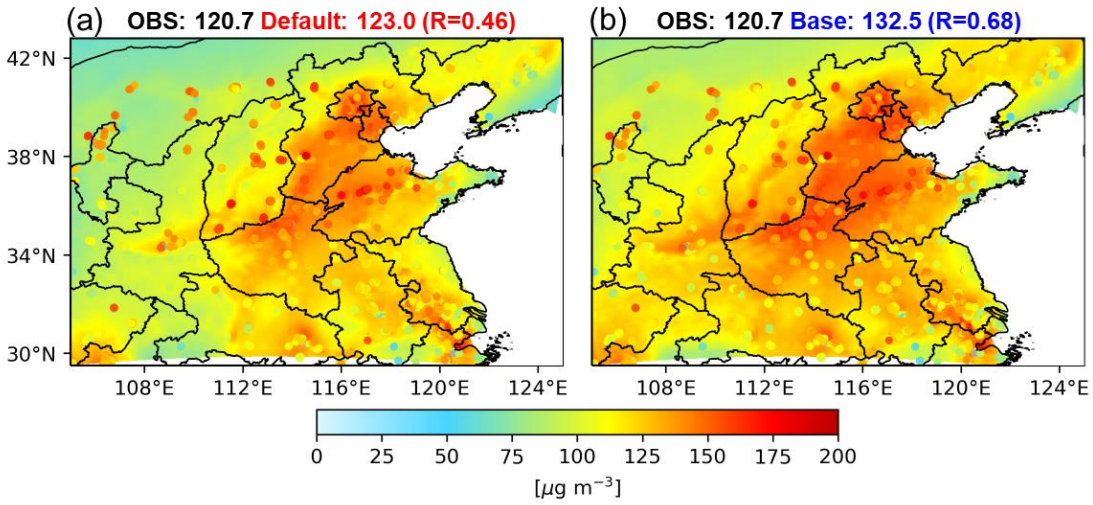

Figure 3. Distribution of observed (dots) and simulated (shaded) surface MDA8 O_3 from (a) Default and (b) Base in North China in July 2018. Statistics in the upper corner of panels are the monthly mean MDA8 O_3 concentrations averaged over the study region and the spatial correlation coefficient R between observations and simulations.

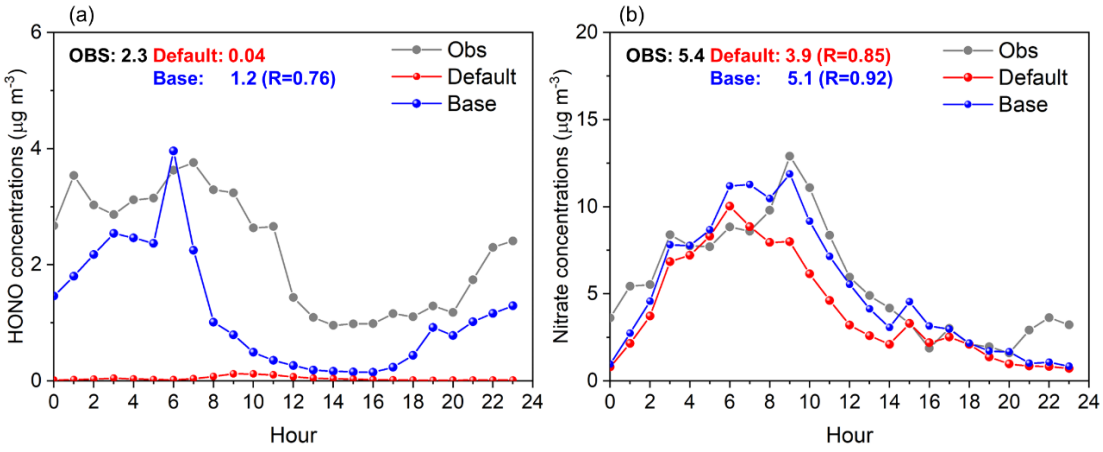

869

870 **Figure 4.** Diurnal variation of observed (in grey) and simulated (Default in red and

871 Base in blue) surface (a) HONO and (b) nitrate concentrations at a rural station in

872 Nanjing in July 2018, with the mean value and temporal correlation coefficients (R)

873 shown in the upper right corner.

874

875

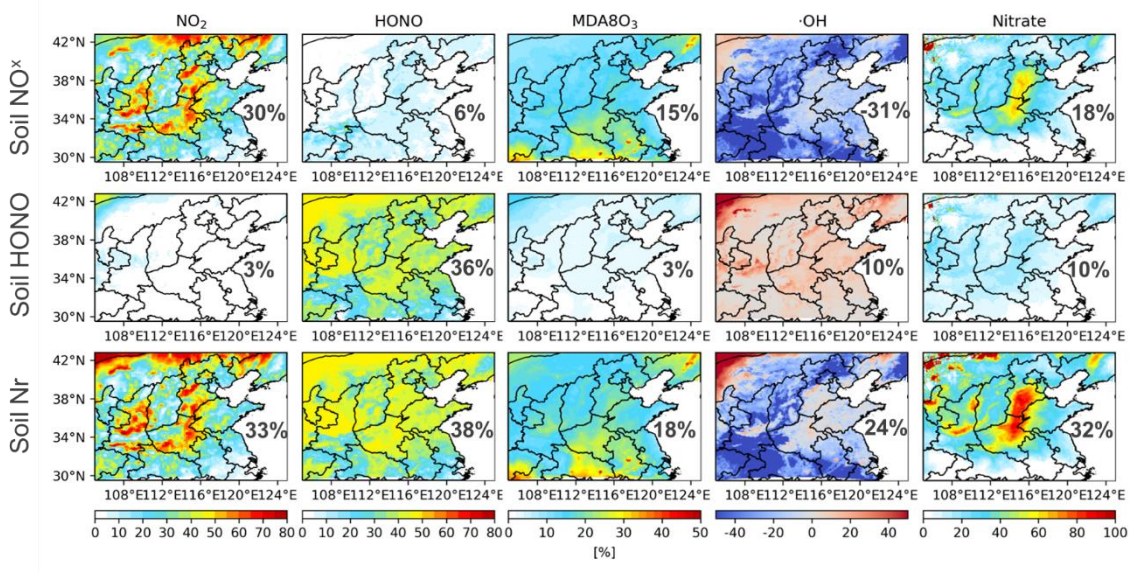

Figure 5. Simulated effects of soil Nr emissions on air quality in North China in July 2018. The first and second rows show the contributions of soil NO_x and soil HONO emissions on monthly average concentrations of NO_2, HONO, $MDA8O_3$, max-1h ·OH, and nitrate, respectively. The third row shows the combined effect of soil Nr emissions on the species listed above. Statistics in the right corner of each panel are the mean values averaged over the study region.

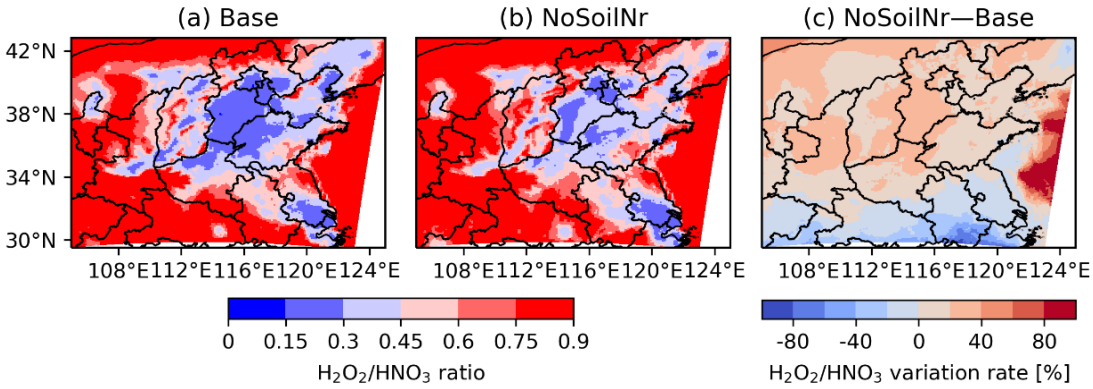

884

885 **Figure 6.** Distribution of the O_3 formation regimes (represented as H_2O_2/HNO_3 ratios)

886 in North China in July 2018 for (a) Base simulation with the addition of soil Nr

887 emissions and (b) NoSoilNr simulation without the addition of soil Nr emissions. (c)

888 Changes in the distribution of O_3 formation regimes due to the soil Nr emissions

889

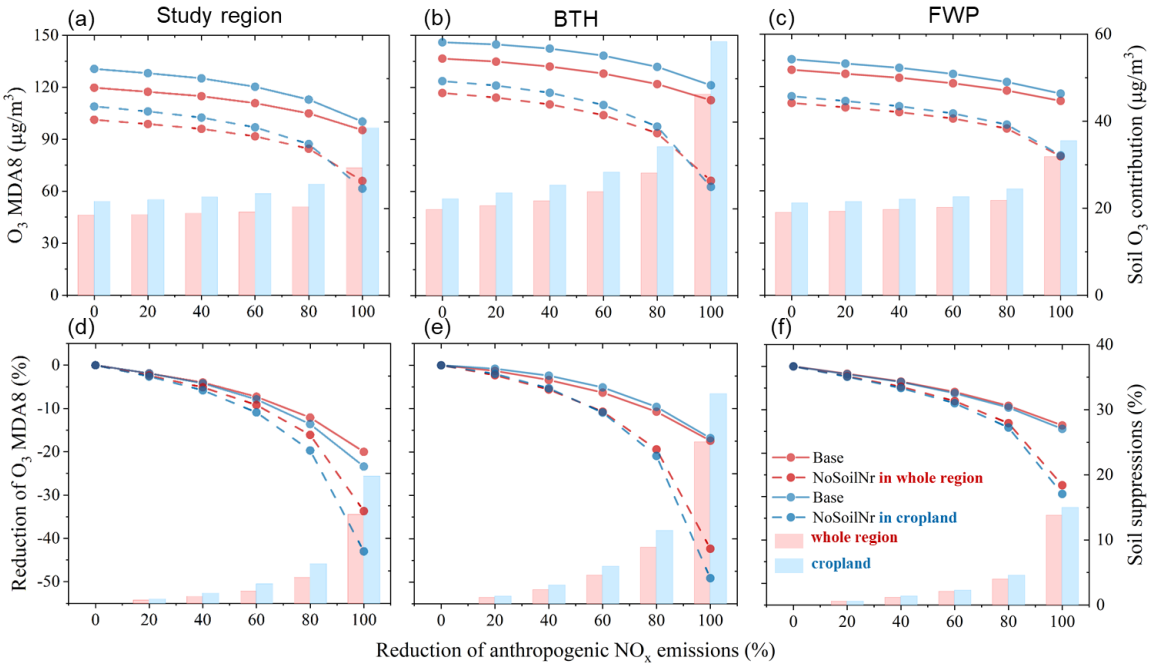

Figure 7. Role of soil Nr emissions in O_3 pollution regulation in North China in July 2018. The responses of MDA8 O_3 concentrations to the reductions of anthropogenic NO_x emissions (20%, 40%, 60%, 80% and 100%) relative to July 2018 levels, in the presence (solid line) and absence (dotted line) of soil Nr emissions in the study region, BTH and FWP region. (The lines in panels a-c and d-f are MDA8 O_3 concentrations and the relative reductions in MDA8 O_3 under different anthropogenic NO_x emission reductions, respectively. The red bars (right y-axis) in panels a-c show the corresponding O_3 contribution from soil Nr emissions, which is determined as the difference between the solid and dotted lines, and the blue bars are the same as the red bars but for statistics in cropland. The red bars (right y-axis) in panels d-f show the suppression of O_3 pollution mitigated due to the existence of soil Nr emissions, which are determined as the difference between the solid and dotted lines, and the blue bars are the same as the red bars but for statistics in cropland.)

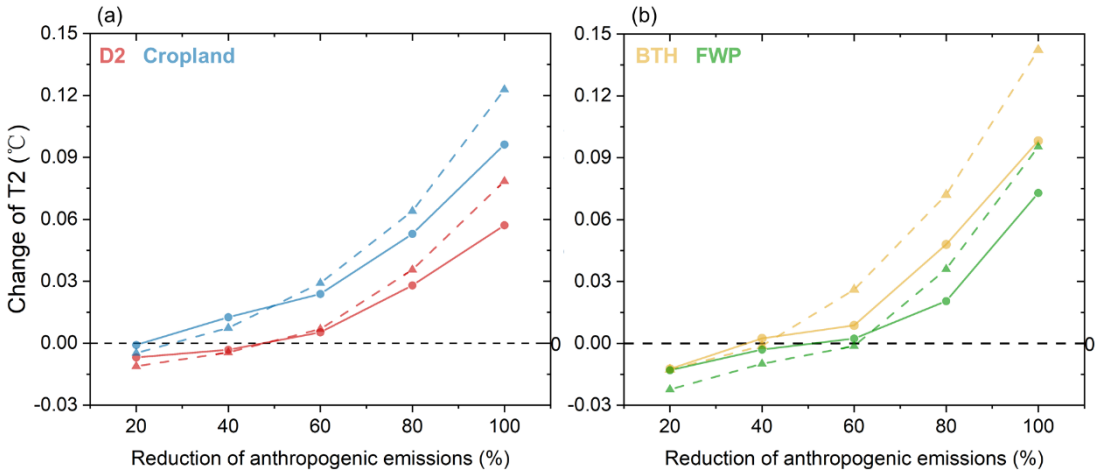

Figure 8. The responses of air temperature at 2m (T2) to the reductions of anthropogenic emissions (taking into accounting the SO_2, NO_x, primary $PM_{2.5}$, VOCs, and CO reduced by 20%, 40%, 60%, 80%, and 100%) relative to July 2018 levels in the presence (solid line) and absence (dotted line) of soil Nr emissions (a) in the study region, (b) BTH and FWP region.